

Equilibration of quantum many-body fast neutrino flavor oscillations

Joshua D. Martin¹,[✉] Duff Neill¹, A. Roggero^{2,3}, Huaiyu Duan⁴, and J. Carlson¹

¹Theoretical Division, Los Alamos National Laboratory, Los Alamos, New Mexico 87545, USA

²Dipartimento di Fisica, University of Trento, via Sommarive 14, I-38123, Povo, Trento, Italy

³INFN-TIFPA Trento Institute of Fundamental Physics and Applications,
via Sommarive 14, I-38123 Povo, Trento, Italy

⁴Department of Physics and Astronomy, University of New Mexico, Albuquerque, New Mexico 87131, USA



(Received 18 August 2023; accepted 31 October 2023; published 7 December 2023)

Neutrino gases are expected to form in high-density astrophysical environments, and accurately modeling their flavor evolution is critical to understanding such environments. In this work, we study a simplified model of such a dense neutrino gas in the regime for which neutrino-neutrino coherent forward scattering is the dominant mechanism contributing to the flavor evolution. We show evidence that the generic potential induced by this effect is nonintegrable and that the statistics of its energy level spaces are in good agreement with the Wigner surmise. We also find that individual neutrinos rapidly entangle with all of the others present, which results in an equilibration of the flavor content of individual neutrinos. We show that the average neutrino flavor content can be predicted utilizing a thermodynamic partition function. A random phase approximation to the evolution gives a simple picture of this equilibration. In the case of neutrinos and antineutrinos, processes like $\nu_e \bar{\nu}_e \leftrightarrow \nu_\mu \bar{\nu}_\mu$ yield a rapid equilibrium satisfying $n(\nu_e)n(\bar{\nu}_e) = n(\nu_\mu)n(\bar{\nu}_\mu) = n(\nu_\tau)n(\bar{\nu}_\tau)$ in addition to the standard lepton number conservation in regimes where off-diagonal vacuum oscillations are small compared to $\nu - \nu$ interactions.

DOI: [10.1103/PhysRevD.108.123010](https://doi.org/10.1103/PhysRevD.108.123010)

I. INTRODUCTION

In hot and dense astrophysical environments such as core collapse supernovae and binary neutron star mergers, neutrinos are emitted in such large number fluxes that the average flavor content is important to the dynamic and chemical evolution. Through weak interactions with local nucleons, electron flavor neutrinos and antineutrinos can alter the local proton-to-neutron ratio in these environments, thereby affecting, for example, r -process nucleosynthesis [1–7]. It is therefore crucial to understand the flavor content of the neutrinos if one wishes to perform detailed studies of the evolution of these systems [8–15].

In regions of high density, neutrinos can undergo coherent forward scattering, which is sensitive to the quantum mechanical flavor state of the neutrino. When scattering on charged leptons, a flavor-dependent relative phase can develop between components of the flavor state. The neutrinos can also exchange flavor content with other neutrinos through neutral current coherent forward scattering. When the number density of neutrinos is sufficiently

large, this flavor exchange effect is expected to dominate the flavor evolution of the neutrino gas, and novel coherent effects such as flavor spectrum splits and swaps may occur [2,8–12,16–18].

In this work, we will study the flavor evolution of such a neutrino gas in the limit that the potential generated by coherent $\nu - \nu$ forward scattering is the dominant effect; this is a regime known in the literature as the “fast” flavor oscillation limit [14,19–33]. In this regime, the redistribution of flavor content among the neutrinos is expected to occur on length scales of approximately a meter. We will study this regime in a quantum many-body formalism with a parametrization of the coherent forward scattering potential which does not impose any simplifying symmetries on the momenta of the neutrinos.

In a core-collapse supernova, the neutrino density is governed by $n_\nu = L/(\bar{E} 4\pi R^2)$. Taking a total luminosity $L = 10^{53}$ erg/sec, $R = 50$ km and an average energy $\bar{E} = 10$ MeV gives a total density $n_\nu \approx 6.6 \times 10^{-7}$ fm⁻³. For a degenerate relativistic Fermi gas, the average energy is given by $\bar{E} = 3E_F/4$, where E_F is the Fermi energy. For a two-species Fermi gas (e and μ flavor neutrinos), the number density is given by $n = E_F^3/(3\pi^2)$. Equating the average neutrino energy to the Fermi energy, we find that the density of a degenerate, zero-temperature two-component Fermi gas is approximately 15 times greater than the above estimated neutrino density. For six neutrino species

Published by the American Physical Society under the terms of the [Creative Commons Attribution 4.0 International license](https://creativecommons.org/licenses/by/4.0/). Further distribution of this work must maintain attribution to the author(s) and the published article's title, journal citation, and DOI. Funded by SCOAP³.

(three neutrino and three antineutrino species) with roughly equal fractions, the density is approximately 45 times lower than a degenerate gas of the same average energy. As we estimate the effects of degeneracy to be minimal, we use Boltzmann statistics for both the neutrinos and antineutrinos. We will also work in the two-flavor approximation such that a single neutrino's flavor quantum state can be written as an SU(2) spinor.

The $\nu - \nu$ coherent forward scattering potential takes the form of an all-to-all Heisenberg-like interaction, and such Hamiltonians are generically expected to be nonintegrable except in special cases. We will provide evidence that this interaction is nonintegrable in the absence of simplifying symmetries and that we observe a characteristic signature of (non)integrability when simplifying symmetries are imposed (relaxed). Furthermore, nonintegrable Hamiltonians are hypothesized to “thermalize” in the sense that expectation values of few-body operators are expected to equilibrate to a value which can be predicted from an appropriate thermodynamic partition function. For the generically parametrized potential, we observe strong agreement between the one-body flavor expectation values obtained in the exact many-body evolution of the system and those predicted from a grand-canonical Boltzmann distribution.

II. ENERGY SPECTRUM

The general Hamiltonian governing the coherent evolution of the neutrino flavor content is composed of three parts (see, e.g., Ref. [34]). The first is the vacuum potential which stems from the fact that the neutrino mass states are linear combinations of flavor states. The second is the matter potential [35,36], and it is generated by coherent forward scattering through charged current interactions with local charged leptons in the environment. Finally, there is the $\nu - \nu$ potential generated through neutral current coherent forward scattering between neutrinos [8,15]. For the rest of this work, we will assume that the vacuum oscillation potential is negligibly small relative to the other two potentials and that its primary effect is to provide perturbation to an otherwise pure flavor product state initial condition. We also assume that the matter profile is uniform in the regions of the environment under consideration, and as such, we may consider a corotating frame to remove its overall effect on each neutrino.

After these modifications, only the $\nu - \nu$ coherent forward scattering Hamiltonian remains. For N neutrinos, it has the form [15]

$$\hat{H}_{\nu\nu} = \frac{\mu}{2N} \sum_{i<j}^N (1 - \mathbf{v}_i \cdot \mathbf{v}_j) \hat{\sigma}_i \cdot \hat{\sigma}_j. \quad (1)$$

Here, $\hat{\sigma}$ is the usual vector of Pauli operators, and $\mu = \sqrt{2}G_{\text{F}}n_\nu$ is the scale of the $\nu - \nu$ interaction. Given a typical core-collapse supernova flux at a radius of 50 km, a simple

estimate gives $\mu \approx 1 \text{ cm}^{-1}$. As it is the only dimensionful parameter in the problem, we hereafter measure all distances and times in units of μ and set $\mu = 1$.

We perform simple numerical simulations for small N in periodic boundary conditions. This is a toy model because an estimate using a typical flux for 20 neutrinos at this density gives a box size of order 300 fm, much too small to be realistic. This is a standard choice in the literature, [13,14,31,37–52] but imposes a great deal more symmetry than a more realistic case. Relaxing this condition would only induce more decoherence in the simulations, a critical ingredient as we discuss below. (For more discussion on the role of decoherence, see, e.g., Refs. [37,38,46,53].)

We will address two commonly employed simplifying symmetries in the literature. The first is the uniform coupling symmetry, under which it is assumed that the $\mathbf{v}_i \cdot \mathbf{v}_j$ term averages to zero under the action of the all-pairs summation in Eq. (1). For this case, the total $H_{\nu\nu}$ is proportional to J^2 and is straightforwardly diagonalized in the absence of the other two relevant potentials. For some choices of one-body potentials, the uniform couplings Hamiltonian may be diagonalized with an algebraic Bethe ansatz [41,51]. This simplification has been well studied, so we will not consider it further.

Another simplifying assumption is to impose an axial symmetry to the velocity coupling term such that the velocity components orthogonal to the momentum symmetry axis (denoted z) average to zero. This is equivalent to making the substitution

$$\hat{H}_{\nu\nu} \rightarrow \hat{H}_{\nu\nu}^{\text{ax}} = \frac{\mu}{2N} \sum_{i<j} (1 - v_{z,i}v_{z,j}) \hat{\sigma}_i \cdot \hat{\sigma}_j. \quad (2)$$

It was recently shown that this symmetry imposition leads to an integrable Hamiltonian which can also be diagonalized with an algebraic Bethe ansatz [52].

There is no known method for systematically diagonalizing the generic Hamiltonian of Eq. (1) through the use of an extensive set of nontrivial conserved charges. A “nontrivial” operator is an operator which is not simply proportional to a projection operator into an eigenstate of the Hamiltonian. The only obvious operators which commute with $\hat{H}_{\nu\nu}$ are the projections of the total angular momentum

$$\hat{J}_a = \frac{1}{2} \sum_{i=1}^N \hat{\sigma}_{a,i} \quad (3)$$

(where $\mathbf{a} \in [1, 3]$ is the vector index of the Pauli matrices) and the square of the total angular momentum ($\hat{J}^2 = \sum_{a=1}^3 \hat{J}_a \hat{J}_a$). Because $\hat{H}_{\nu\nu}$ commutes with \hat{J}^2 , \hat{J}_3 , and the ladder operators \hat{J}_\pm , the energy eigenstates can only be linear combinations of $|j, m\rangle$ in these degenerate subspaces. To obtain a the full energy spectrum, one can “brute force” diagonalize $\hat{H}_{\nu\nu}$ in the lowest $|m|$ subspace for each j . Because $\hat{H}_{\nu\nu}$ commutes with the angular momentum ladder

operators, the energy spectrum is $2j + 1$ -fold degenerate for each j , and eigenstates with higher values of $|m|$ can be systematically constructed from the minimal $|m|$ states with suitable applications of the ladder operators.

In the following, we construct the Hamiltonian by first drawing the z components of the velocities on the interval $v_z \in [-1, 1]$ randomly from a Gaussian-like distribution centered on $v_z = 1$ with a standard deviation of $1/2$ such that $P(v_z) \propto e^{-2(v_z-1)^2}$. We choose this distribution to approximate the forward-peaked-ness of the neutrino momenta emitted from the proto-neutron star surface. For the axially symmetric case, the x and y components are chosen to be identically zero. For $\hat{H}_{\nu\nu}$, which retains all three components of the unit velocities, we choose $v_x = \sqrt{1 - v_z^2} \cos(\phi)$ and $v_y = \sqrt{1 - v_z^2} \sin(\phi)$, where ϕ is a chosen to be a random number uniformly drawn in the interval $[0, 2\pi]$.

Finally, we will solely treat the evolution of initial product states. This necessarily assumes that the neutrinos entering a given region of space have developed a negligible correlation in their flavor evolution prior to the interaction we consider herein. We make this approximation only in the interest of analyzing the salient dynamics of the evolution under $\hat{H}_{\nu\nu}$. More careful treatment of the initial state will require a detailed study of the neutrino-neutrino self-interaction in the presence of non-negligible momentum changing scattering processes in the dense matter of the proto-neutron star core.

A. Level spacings

We next consider the structure of the spectrum of $\hat{H}_{\nu\nu}$ in its m and j symmetry sectors. In each sector, we sequentially order the energy eigenvalues and investigate the differences between the sequential energies which we denote $s_\alpha \equiv (E_{\alpha+1} - E_\alpha)/\bar{s}$, where \bar{s} is chosen such that the average over the energy differences is unity.

Integrable systems are characterized by an extensive set of (nontrivial) operators which commute with the Hamiltonian, and these conserved quantities permit substantial degeneracy in the energy spectrum. When considering the sequential energy differences for an integrable system, the probability of two sequential energy eigenvalues having spacing s is a Poisson distribution, $P(s) = e^{-s}$. In contrast, nonintegrable Hamiltonians demonstrate repulsion between energy levels, and the probability distribution for spacing s is, in accordance with the Wigner surmise, of the form $P(s) = \frac{\pi}{2} s e^{-\pi s^2/4}$ for a Gaussian orthogonal ensemble (GOE) [54].

When extracting the distribution of energy differences from a particular Hamiltonian, an unfolding procedure must be performed in order to approximately remove the effect arising from the fact that the Hamiltonian has a finite density of states which may be sparser in some energy regions than others [55]. Instead of considering directly the

distribution of level differences s_i , one can consider the probability distribution for the ratio of sequential level differences, defined as $r_\alpha \equiv \frac{s_{\alpha+1}}{s_\alpha}$, which is insensitive to the local density of states. The new probability distribution, $P(r)$, for the integrable (Poisson) case is

$$P(r) = \frac{1}{(1+r)^2}, \quad (4)$$

while for nonintegrable (GOE) cases, $P(r)$ is

$$P(r) \approx \frac{27}{8} \frac{r(1+r)}{(1+r(1+r))^{\frac{5}{2}}}. \quad (5)$$

For the GOE case, the expression in Eq. (5) was derived as an exact expression for 3×3 random matrices drawn from a Gaussian orthogonal ensemble. It is in good agreement with numerical studies of larger random matrices, and the correction derived from fits to numerical distributions extracted from larger random matrices can be found in Ref. [55]. The approximate correction for the large matrix case is $\mathcal{O}(10^{-2})$ and is not visible on the scale plotted in Fig. 1.

In Fig. 1, we compare the distribution of r_i for the two Hamiltonians we have discussed. The Hamiltonian, $\hat{H}_{\nu\nu}$, implements generic unit magnitude three velocities, while the axially symmetric (abbreviated ‘‘ax’’) Hamiltonian, $\hat{H}_{\nu\nu}^{\text{ax}}$, implements the identical $v_{z,i}$ values as $\hat{H}_{\nu\nu}$ but takes the x and y components of the velocities equal to zero by construction. As previously mentioned, $\hat{H}_{\nu\nu}^{\text{ax}}$ is known to be integrable, and therefore the level spacings in its spectrum are expected to obey Poisson-like statistics.

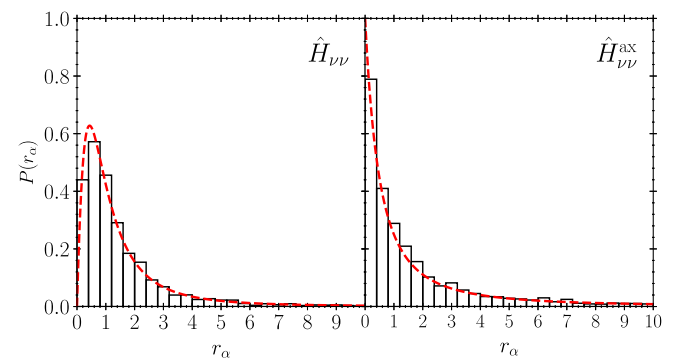


FIG. 1. Extracted statistics (black histogram) for the ratio of sequential level spacings of the Hamiltonian for the nonintegrable generic parametrization ($\hat{H}_{\nu\nu}$, left panel) and for the integrable axially symmetric simplification ($\hat{H}_{\nu\nu}^{\text{ax}}$, right panel) for $N = 16$ in the $j = 2$, $m = 2$ subspace. Overlaid as a red dashed line is the predicted probability distribution for the ratio of sequential level spacings for the nonintegrable (GOE, left panel) distribution and the integrable (Poisson, right panel) distribution.

TABLE I. Average ratios of consecutive level spacings for $\hat{H}_{\nu\nu}$ and $\hat{H}_{\nu\nu}^{\text{ax}}$ of 16 neutrinos in the subspaces with $j = 0, \dots, 4$ and $m = 0$ which have 1430, 3432, 3640, 2548, and 1260 energy levels, respectively.

j	0	1	2	3	4
$\bar{r}(\hat{H}_{\nu\nu})$	1.6651	1.7126	1.7512	1.7707	1.8508
$\bar{r}(\hat{H}_{\nu\nu}^{\text{ax}})$	3.7211	3.7741	3.8224	3.6091	3.8764

For both cases, we use 16 neutrinos in the construction of the Hilbert space.

We diagonalize $\hat{H}_{\nu\nu}$ and $\hat{H}_{\nu\nu}^{\text{ax}}$ in the $j = 2$ subspace and plot the normalized histogram of ratios of level spacings (r_α). We also compare directly with the expected universal probability distributions for the integrable and nonintegrable cases. This figure provides evidence that the generically parametrized Hamiltonian does not have an extensive set of “hidden” conserved charges corresponding to some hitherto unrecognized symmetry.

To validate that the level spacing statistics in the other j subspaces behave similarly, we compute the average \bar{r}_α with respect to the extracted probability distribution and show the results for $j \leq 4$ in Table I. The distribution of ratios of level spacings should not depend on the subspace, so this average value should take a universal value. For the GOE case, it can be shown that the value is $\bar{r}_\alpha \approx 1.7789$ (see Table 1 of Ref. [55]). However, for the Poisson case, the average diverges as $r_\alpha \rightarrow \infty$, so for any finite distribution of level spacings, the average can take arbitrary and unbounded values.

III. ENERGY DEPHASING

The distribution of the ratio of level spacings is in good agreement with the probability distribution one would expect if the Hamiltonian under consideration were a random matrix drawn from a GOE. The level repulsion resulting from a lack of an extensive set of symmetries implies that energy differences should not be expected to vanish for the bulk of states in the spectrum. Furthermore, the effective random nature of the Hamiltonian implies that differences in energies should not generically be simple rational numbers. As such, the time-dependent phases of off-diagonal matrix elements of operators in the energy basis should be expected to individually average to zero over arbitrary time windows after the state has evolved for a sufficiently long time. Thus, under a time average over an arbitrary interval at late time, the expectation value of $\hat{\sigma}_{3,i}$ should be in good agreement with the value predicted by computing the average with respect to the incoherent energy diagonal distribution which preserves the energy state probabilities of the initial condition. Thus, we will compute and compare the approximation

$$\begin{aligned} \frac{1}{\Delta} \int_{t_{\text{eq}}}^{t_{\text{eq}}+\Delta} dt \langle \hat{\sigma}_{3,i} \rangle(t) &= \frac{1}{\Delta} \int_{t_{\text{eq}}}^{t_{\text{eq}}+\Delta} dt \sum_{E,E'} e^{-i(E-E')t} \langle E | \psi_0 \rangle \\ &\quad \times \langle \psi_0 | E' \rangle \langle E' | \hat{\sigma}_{3,i} | E \rangle \\ &\approx \sum_E |\langle E | \psi_0 \rangle|^2 \langle E | \hat{\sigma}_{3,i} | E \rangle, \end{aligned} \quad (6)$$

where $|\psi_0\rangle$ represents the initial quantum state and $t_{\text{eq}} > 1/\mu$ is the (as yet unknown) time it takes for the system to reach its equilibrium value. The time window $[t_{\text{eq}}, t_{\text{eq}} + \Delta]$ must also be selected such that the oscillations due to the coherent evolution of the quantum system about the average expectation value can be fully captured. We will refer the value t_{eq} as the equilibration timescale, and we will discuss our observations of it in the next section. We refer to the incoherent probability weighted sum of operator expectation values in the final line of Eq. (6) as the energy mixed state distribution (EMSD).

A. Thermalization

Nonintegrable many-body Hamiltonians are widely expected to obey the so-called Eigenstate Thermalization Hypothesis (ETH) [56–58]; see Ref. [59] for a review. Many numerical studies of ETH have been conducted, and we refer to Refs. [60–62] as a very incomplete list of examples for when the system has an underlying lattice structure. For systems with all-to-all interactions or no discernible lattice structure, there is a less extensive literature, and we refer to Refs. [63–65] as examples. Besides integrable systems, for a generic Hamiltonian, ETH may only hold for the majority of the eigenstates. Certain eigenstates (quantum scars) embedded in the spectrum may have additional symmetries beyond that of the Hamiltonian, invalidating ETH for that state; see, for instance, Refs. [66,67]. However, these states are expected to have measure zero in the density of states in the thermodynamic limit, unless there is special symmetry protection. Loading the Hamiltonian with additional symmetry, while not inducing integrability, results in the fracturing of the Hilbert space into many block-diagonal subsectors, with each subspace being simply too small for ETH [68].

The ETH is fundamentally a statement about the structure of “few-body” operators that act on a subextensive number of the local Hilbert spaces that tensor together to form the full many-body Hilbert space. For a few-body operator \hat{O} , the matrix element between two eigenstates $|E_\alpha\rangle, |E_\beta\rangle$ of the Hamiltonian is hypothesized to be given by the ansatz,

$$\begin{aligned} \langle E_\alpha | \hat{O} | E_\beta \rangle &= \hat{O}(E_{\text{ave}}) \delta_{\alpha\beta} \\ &\quad + e^{-S(E_{\text{ave}})/2} f_{\hat{O}}(E_{\text{ave}}, \omega_{\alpha\beta}) R_{\alpha\beta}, \end{aligned} \quad (7)$$

$$S(E_{\text{ave}}) = \ln \sum_{\alpha} E_{\alpha} \delta_{\epsilon}(E_{\text{ave}} - E_{\alpha}). \quad (8)$$

where $E_{\text{ave}} = \frac{E_\alpha + E_\beta}{2}$, and $\omega_{\alpha\beta} = E_\alpha - E_\beta$. $\hat{O}(E_{\text{ave}})$ is the microcanonical average of the operator \hat{O} over states near E_{ave} , and S is the suitable microcanonical entropy, counting the number of eigenstates near E_{ave} within a small window given by ϵ . $R_{\alpha\beta}$ is an independent random number for each α, β with average zero but variance 1. When the dimension of the total Hilbert space is large, we can expect S to be large even for very narrow windows, so in the thermodynamic limit, we can take $\epsilon \rightarrow 0$ and have the matrix element of the operator in eigenstates be dominated by the microcanonical average. Finally, the function f_δ is related to the linear response correlation function of the thermodynamic system when perturbed by the operator \hat{O} [69] and, for fixed E_{ave} , decreases exponentially in the energy difference $\omega_{\alpha\beta}$ for such chaotic systems (see, e.g., Refs. [70,71]).

In general, we expect the ETH ansatz [Eq. (7)] for the matrix elements to hold for a chaotic system but not for an integrable one. As shown above, the neutrino Hamiltonian $\hat{H}_{\nu\nu}$ in Eq. (1) we use can reproduce both behaviors depending on the choice of the velocities. To test the validity of ETH for our problem, we consider matrix elements of $\hat{\sigma}_{3,i}$ on the first neutrino in both the integrable and nonintegrable regimes. We first show the diagonal matrix elements $\langle E_\alpha | \hat{O} | E_\alpha \rangle$ in Fig. 2 for both the integrable (red data in the right panel) and nonintegrable case (blue data in the left panel). One can see that in the former (integrable) case the diagonal matrix element has large fluctuations over nearby frequencies throughout the whole spectrum, while for the nonintegrable case, the expectation value in the bulk of the spectrum is approximately a function of energy alone as expected from the ansatz in Eq. (7). Next, in Fig. 3, we show the magnitude of the off-diagonal matrix elements of $\hat{\sigma}_{3,i}$ on the first neutrino as a function of the energy difference $|\omega_{\alpha\beta}|$ for all states in a narrow energy window of size $\epsilon = 0.005[\mu]$ around an average energy E_{ave} in the middle of the spectrum; for the

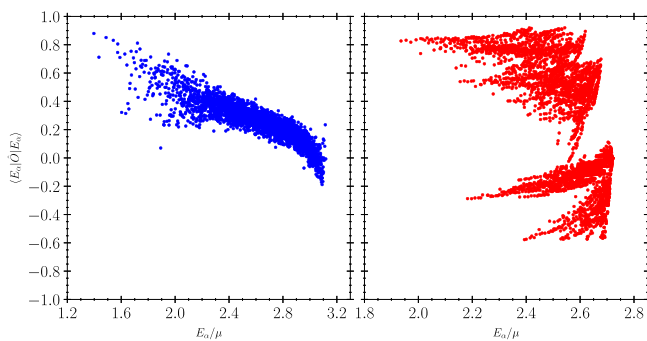


FIG. 2. Diagonal matrix elements $\langle E_\alpha | \hat{O} | E_\alpha \rangle$ with $\hat{O} = \hat{\sigma}_3$ on the first neutrino in the energy eigenbasis as a function of the energy E_α (in units of μ). The left panel shows results for the nonintegrable Hamiltonian $\hat{H}_{\nu\nu}$, while the right panel shows results for the integrable case $\hat{H}_{\nu\nu}^{\text{ax}}$; in both cases, we only look at the $j = 2$ and $m = 2$ subspace.

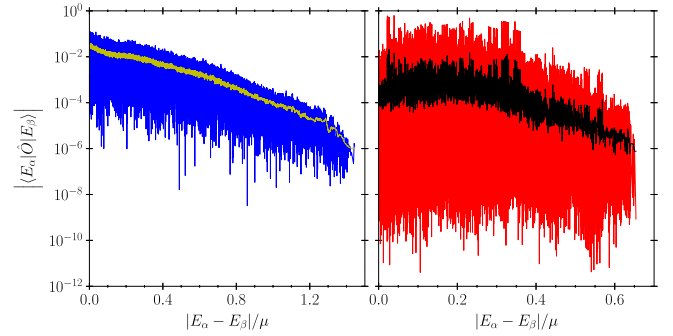


FIG. 3. Magnitude of the off-diagonal matrix elements $|\langle E_\alpha | \hat{O} | E_\beta \rangle|$ with $\hat{O} = \hat{\sigma}_3$ on the first neutrino in the energy eigenbasis as a function of the absolute value of the energy difference $|E_\alpha - E_\beta|$ (in units of μ). The left panel shows results for the nonintegrable Hamiltonian $\hat{H}_{\nu\nu}$ (blue data), while the right panel shows results for the integrable case $\hat{H}_{\nu\nu}^{\text{ax}}$ (red data); in both cases, we only look at the $j = 2$ and $m = 2$ subspace. Also shown is the running average of the matrix elements' magnitude obtained taking the median over a window of 50 matrix elements (yellow curve on the left panel and black curve on the right panel).

results shown here, we took $E_{\text{ave}} = 2.4[\mu]$. One can clearly see an exponential decay for large energy difference in the nonintegrable case (left panel), while for the integrable model (right panel), the size of the off-diagonal matrix elements fluctuates by more than 6 orders of magnitude for every value of $|\omega_{\alpha\beta}|$. To better visualize the importance of a large number of outliers in the integrable case, which are instead not present in the nonintegrable system on the left, we also report in Fig. 3 the running average of the matrix element size obtained by taking the median over a window of 50 matrix elements. This is a direct estimate of the absolute value of the function $f_\delta(E, \omega)$ in Eq. (7) for E in the middle of the spectrum (cf. Refs. [59,72]).

All results shown in Figs. 2 and 3 were obtained for a system with $N = 16$ neutrinos and for states restricted to $j = 2$ and $m = 2$ subspace.

The basic intuition behind eigenstate thermalization is that few-body operators are unable to distinguish which eigenstate the system is in, with nearby (in energy) eigenstates displaying similar few-body behavior. When the dimension of the Hilbert space becomes large, the eigenstate thermalization is often described using canonical or grand-canonical ensembles, since the expectation values are expected to be effectively equal in either ensemble. When using the (grand-)canonical ensemble, the temperature (or other chemical potentials) are tuned to match the energy and other quantum numbers of the desired eigenstate of the system. After this, the matrix elements of generic few-body operators can be computed in the appropriate thermal ensembles. When ETH holds, we can effectively claim that up to small corrections the time-averaged spectrum of few-body operators “thermalize” even in a single eigenstate and

are thus computable from thermal ensembles. One can generalize the eigenstate thermalization to any state of the system, provided the expectation value of the variance of the energy for that state is appropriately small.

If our system thermalizes in this sense, then we can predict the (time-averaged) expectation value of the individual neutrinos at large times utilizing a grand-canonical statistical distribution. As the system is time independent, and \hat{J}_3 and \hat{J}^2 commute with the Hamiltonian, we construct a partition function using one temperature parameter (β) and two chemical potentials (μ_3 and μ_2). For a given initial condition, we find these parameters by fitting the expectation values of the relevant operators calculated using the partition function to the invariant expectation values calculated with respect to the initial condition. This amounts to finding β , μ_3 , and μ_2 such that

$$\langle \psi_0 | \hat{O} | \psi_0 \rangle = \frac{1}{\mathcal{Z}} \text{Tr}(\hat{O} e^{-\beta \hat{H}_{\nu\nu} + \mu_3 \hat{J}_3 + \mu_2 \hat{J}^2}) \quad (9)$$

for the conserved quantities $\hat{O} = \hat{H}_{\nu\nu}, \hat{J}_3, \hat{J}^2$ and $\mathcal{Z} = \text{Tr}(e^{-\beta \hat{H}_{\nu\nu} + \mu_3 \hat{J}_3 + \mu_2 \hat{J}^2})$ is the partition function. Once the temperature and chemical potentials have been determined, the (time-averaged) expectation value of the flavor content for a given neutrino (i) can be predicted by computing $\langle \hat{\sigma}_{3,i} \rangle \approx \text{Tr}(\hat{\sigma}_{3,i} e^{-\beta \hat{H}_{\nu\nu} + \mu_3 \hat{J}_3 + \mu_2 \hat{J}^2})$.

We next investigate the late-time behavior of an example product state initial condition for 16 neutrinos. We employ the same couplings in $\hat{H}_{\nu\nu}$ as in the previous sections, and we order them from lowest to highest value of $v_{z,i}$ in increasing values of the particle index $i \in [1, 16]$. We next choose the first $i \in [1, \lfloor N/2 \rfloor + 1]$ neutrinos to be electron flavor (corresponding to the lowest 9 v_z values for 16 neutrinos) and the remaining (highest v_z) neutrinos to be τ flavor. Finally, to mimic the effects of the neglected one-body contributions to the Hamiltonian, we perturb the initial flavor configuration by a small random polar rotation away from initial pure flavor states as well as a random rotation in the x - y plane of the flavor Bloch sphere. The first rotation mimics the effect of the small effective mixing angle induced by noncommutation of the dense matter and vacuum potentials, while the second rotation mimics the phase accumulation from the rapid rotations about the flavor axis induced by the matter potential.

Once the couplings and initial conditions are specified, we then evolve the 16 neutrino quantum state by numerically solving the many-body Schrödinger equation in the interval $t = [0, 10^3] \mu^{-1}$. Using the time-evolved quantum state, we compute the average of $\langle \hat{\sigma}_{3,i} \rangle$ over the interval $t = [10^1, 10^3] \mu^{-1}$. We show this time-averaged quantity in the top panel of Fig. 4 and we compare time-averaged numerical predictions for $\langle \hat{\sigma}_{3,i} \rangle$ with the mixed state predictions for each spin. The red squares represent the time-averaged values of the evolved quantum state, and the green circles (blue diamonds) show the expectation value

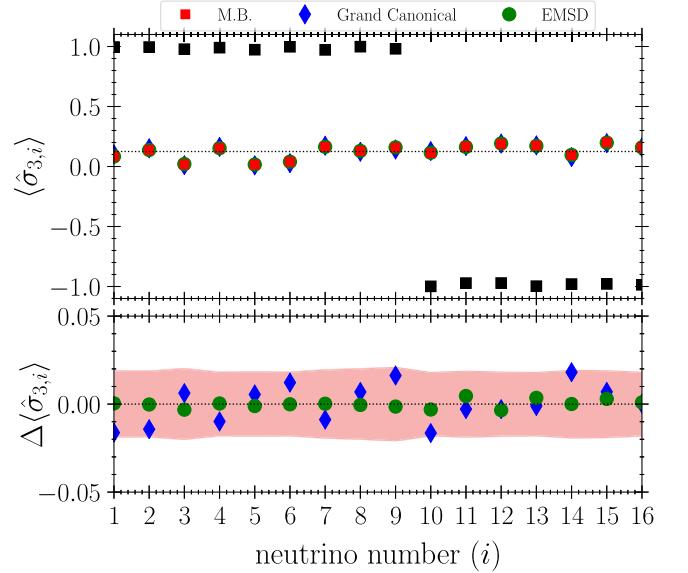


FIG. 4. In the top panel, we show the initial condition (black squares) and the average over the late-time oscillations of $\langle \hat{\sigma}_{3,i} \rangle$ obtained from the solution to the many-body Schrödinger equation for each neutrino. The thin black dotted line indicates the conserved value $2\langle \hat{J}_3 \rangle / N$. Blue diamonds are the expectation value predicted from the grand-canonical partition function fit from the initial condition, while green circles indicate the EMSD average. The lower panel shows the difference ($\Delta \langle \hat{\sigma}_{3,i} \rangle$) between the exact solution and the partition function fit (blue diamond) and the numerical solution to the MB Schrödinger equation and the microcanonical approximation (green circles). The filled red area represents the RMS deviation of the oscillations of the exact solution about its mean.

estimated using the EMSD (grand-canonical) approximation of Eq. (6) [Eq. (9)]. The bottom panel shows the difference between the late-time averaged many-body solution and the two energy diagonal predictions, while the filled red region indicates the root-mean-square (RMS) deviation of the time oscillations of the expectation value of the many-body solution about its mean (as seen in Fig. 5). We observe that both of the energy diagonal approximations for the estimation of $\langle \hat{\sigma}_{3,i} \rangle$ are fully within the RMS oscillations of the many-body solution about its mean, except one outlying point estimated using the grand-canonical ensemble.

It is important to note that, while the interaction is $SU(2)$ invariant, we choose a particular spin direction along which to quantize (which is informed by the initial polarization) and denote it as \vec{e}_3 . Because $\hat{H}_{\nu\nu}$ commutes with \hat{J}_+ and \hat{J}_- , their expectation values are also conserved, but these operators cannot be simultaneously diagonalized with \hat{J}_3 and \hat{J}^2 . Therefore, no mixed state which is *energy diagonal* will be able to accurately predict their expectation values. For the initial conditions we consider here, $\langle \hat{J}_+ \rangle \approx \langle \hat{J}_- \rangle \approx 0$. As such, the energy-diagonal mixed states we consider here are adequate for describing the

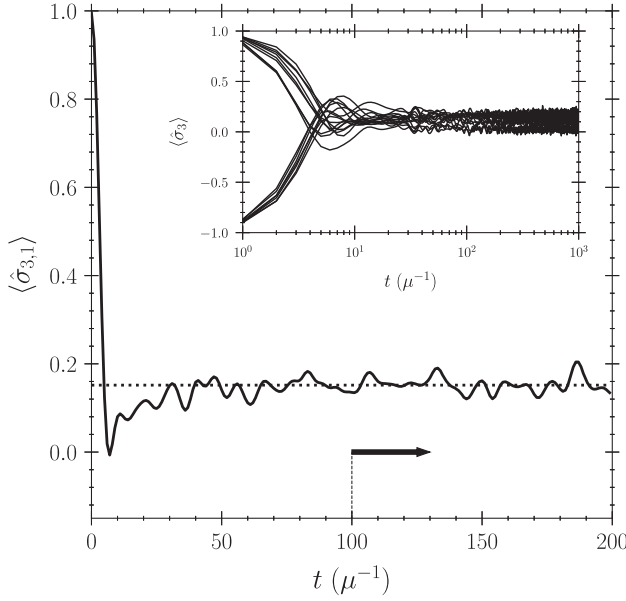


FIG. 5. Evolution of $\langle \hat{\sigma}_3 \rangle$ for neutrino $i = 1$ compared to the prediction utilizing the grand-canonical partition function (black dotted line) at early time. The line and arrow indicate when the time-averaging begins for the evaluation of the data plotted in Fig. 4. Inset: $\langle \hat{\sigma}_3 \rangle$ as a function of time for every neutrino on the entire considered time domain.

polarization configurations. However, in the presence of substantial orthogonal polarization (i.e., substantially non-zero values of $\langle \hat{J}_\pm \rangle$), a more careful treatment of the non-Abelian conserved charges would be necessary [73].

B. Approach to equilibrium

In the previous sections, we have argued that in the absence of simplifying symmetries the $\nu - \nu$ interaction Hamiltonian in its various symmetry sectors has a level spacing distribution which is in good agreement with that of a random Hamiltonian drawn from the GOE. We have also argued that this implies generic product state initial conditions should display substantial dephasing in energy such that one-body expectation values can be computed from an energy-diagonal distribution. Once dephased, the one-body expectation values are expected to achieve an equilibrium value from which they stray only transiently and with small amplitude.

To investigate the approach to this equilibrium, we evolved seven different systems each with N spins from $N = 10$ to $N = 16$ in integer steps. For each system size, we independently selected velocities and initial conditions in the same manner as described for the $N = 16$ case shown in detail above. We then considered three simple measures of the speed of the evolution. First, for each system size (N), we consider the one-body von Neumann entropy [$S_i = -\text{Tr}(\rho_i \log_2(\rho_i))$] of each neutrino, and we find the earliest time for which $S_i > 0.95$. We then take the average

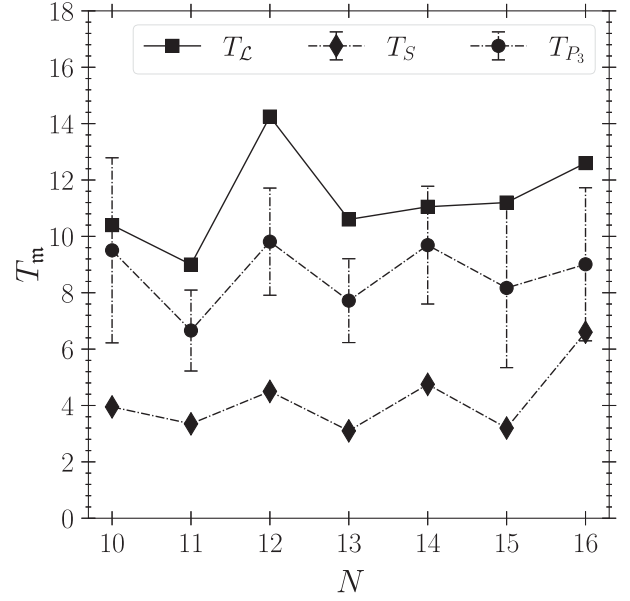


FIG. 6. Times for which the average time (T_S , indicated by black diamonds) the one-body entropies reach 95% of their maximum, the Loschmidt echo (T_L , black squares) reaches its first local minimum, and the average time (T_{P_3} , indicated by black circles) the one-body $\langle \hat{\sigma}_3 \rangle$ reaches its first turning point.

of these times over all the spins for a given system size, denote this average large entropy time as T_S , and plot T_S as black diamonds in Fig. 6. We also computed the standard deviation of T_S over the spins for each system size; however, in each case, the error bar would be too small to resolve on the plotted scale of Fig. 6.

Next, we note the time dependent behavior Fig. 5 of $P_3 \equiv \langle \hat{\sigma}_3 \rangle$. After evolving away from the initial value, the expectation value crosses the thermal prediction before turning and approaching it again. We observe this behavior across all of the chosen system sizes and for each spin. We therefore consider, for each system size, the time at which the value $\langle \hat{\sigma}_3 \rangle$ for each spin reaches a turning point at which its first time derivative vanishes. We then average these turning-point times over all the spins, denote the average time as T_{P_3} , and plot it as black circles in Fig. 6, and we indicate the standard deviation from the average value over the spins in a given system size with error bars.

Finally, we consider the Loschmidt echo $\mathcal{L}(t) = |\langle \psi_0 | e^{-i\hat{H}_{\nu\nu}t} | \psi_0 \rangle|^2$ which quantifies the probability of measuring the time-evolved state in the initial configuration. The $t = 0$ curvature of the Loschmidt echo is given by the variance of the Hamiltonian, and the earliest time at which it (the Loschmidt echo) can vanish is bounded by the quantum speed limit [74]. For chaotic systems, the Loschmidt echo is expected to saturate to an equilibrium value which scales inversely proportionally to the size of the system's Hilbert space [75], a scaling behavior that we have verified for $\hat{H}_{\nu\nu}$. The dynamics of the echo at intermediate times is an active area of study, but we

investigate the time of the first minima in the echo as a proxy to the equilibration timescale of the system.

For all of the calculations we have performed, we have observed an approach to an equilibrium value in the one-body flavor content with a timescale which appears insensitive to the total number of spins. The equilibration we observe in flavor content is subsequent to a development of one-body entanglement on a timescale which is similarly insensitive to N . Our numerical observations are consistent with a time-to-equilibrium which scales simply as $\mathcal{O}(\mu^{-1})$. In Fig. 6, we show the timescales we extracted for the equilibration of these quantities for a range of system sizes. Because our computational method retains all amplitudes, we are computationally limited in the system sizes N we can investigate.

For states that are close to polarized product states in the \vec{e}_3 direction, we can argue that the timescale to equilibrium cannot scale to zero as $N \gg 1$. In the Appendix, we calculate to quadratic order in the Taylor series expansion of the time evolution of $\langle \hat{\sigma}_{3,i}(t) \rangle$ about $t = 0$. We find that, for the typical states we consider here, the linear term in the expansion vanishes, and the quadratic term scales as μ^2/N . We expect such a Taylor series to have a radius of convergence scaling as μ^{-1} . Noting $\langle \hat{\sigma}_{3,i}(t = 0) \rangle \approx \pm 1$, then truncating the series at quadratic order, and estimating when $\langle \hat{\sigma}_{3,i}(t) \rangle \approx 2\langle \hat{J}_3 \rangle/N \ll 1$, we would conclude $t \sim \sqrt{N}/\mu$. However, such a timescale is outside the expected region of convergence for our series, making such a conclusion not self-consistent. We can, though, conclude that $t \rightarrow 0$ as $N \gg 1$ is impossible; the smallness of the quadratic term, and the suppression of higher orders as $t \rightarrow 0$, would not allow a self-consistent solution to the equilibrium condition in arbitrarily small neighborhoods of the origin. We intend to follow up these observations with investigations of these timescales both analytically and with computational methods which may allow substantially larger system sizes, such as tensor network methods.

C. Path integral description of time evolution and equilibrium distributions

In the results presented in the previous section, it is striking that at late times each individual neutrino flavor expectation value is approximately given by $\langle \hat{\sigma}_{3,i} \rangle \approx 2\langle \hat{J}_3 \rangle/N$. We observe this approximate flavor isotropy even when there is substantial correlation between the initial flavor content and momenta of the neutrinos (as in the initial split configuration of Fig. 4). This is behavior we have observed across a variety of system sizes and initial correlations between flavor and momenta. The total $\langle \hat{J}_3 \rangle$ is, of course, conserved by the Hamiltonian, but there is no *a priori* reason to expect all the spins to reach the same equilibrium value. To clarify this point and to define the equilibrium values for general systems of neutrinos (and both neutrinos and antineutrinos), we consider the time evolution in a path integral approach.

The time-evolved expectation value of an operator expressed as an expansion of overlaps with the initial state for a system described by the GOE produces random phases in the off-diagonal elements that would normally be present in Eq. (6). Rewriting the expectation value as a sum over product states of ν_e and ν_τ spins $|n\rangle$, the amplitude of the state in state $|n\rangle$ as a function of time is

$$\langle n|\psi(t)\rangle = \sum_{\alpha} e^{-iE_{\alpha}t} \langle n|E_{\alpha}\rangle \langle E_{\alpha}|\psi_0\rangle, \quad (10)$$

where we have taken the initial state $|\psi_0\rangle$ as an arbitrary state in the $|n\rangle$ basis.

Equivalently, writing the state $|\psi(t)\rangle$ as a sum over the states $|n\rangle$,

$$|\psi(t)\rangle = \sum_n A_n(t) e^{i\phi_n(t)} |n\rangle, \quad (11)$$

where the $A_n(t)$ are the magnitudes of the overlaps (real and positive) and the phases are $\phi_n(t)$. The magnitudes and phases are given by

$$A_n(t) e^{i\phi_n(t)} = \sum_{\alpha} e^{-iE_{\alpha}t} \langle n|E_{\alpha}\rangle \langle E_{\alpha}|\psi_0\rangle. \quad (12)$$

The expectation value of $\hat{\sigma}_{3,i}$ averaged over a time window of size Δ is

$$\begin{aligned} & \frac{1}{\Delta} \int_t^{t+\Delta} dt \langle \psi(t) | \hat{\sigma}_{3,i} | \psi(t) \rangle \\ & \approx \sum_{n,\alpha} \langle n | \hat{\sigma}_{3,i} | n \rangle | \langle n | E_{\alpha} \rangle \langle E_{\alpha} | \psi_0 \rangle |^2, \end{aligned} \quad (13)$$

and we have used the facts that $\hat{\sigma}_{3,i}$ is diagonal in the $|n\rangle$ basis and that the average over nondiagonal energy eigenstates over time goes to zero. This is a sum over diagonal matrix elements in the $|n\rangle$ basis, each with a positive coefficient, suggesting the time-evolved state can be written as an incoherent sum of the states $|n\rangle$.

For an initial state with overlaps with many eigenstates, the random phases ($e^{-iE_{\alpha}t}$) for a GOE would translate to random phases in the $\nu_e - \nu_\tau$ product state basis $\phi_n(t)$. This would not be true near the ground state where the phases cannot be random, but initial product states we wish to describe are not near the ground state of this Hamiltonian. Random phases also keep $\langle \hat{\sigma}_{\pm,i} \rangle = \langle \hat{\sigma}_{\mp,i} \rangle = 0$ for all times for an initial product state in $|n\rangle$.

The Hamiltonian can always be divided into diagonal ($\hat{H}_{\nu\nu}^d$) and off-diagonal ($\hat{H}_{\nu\nu}^{\text{od}}$) pieces, where, in the $|n\rangle$ basis, the off-diagonal pieces are proportional to $(1 - \mathbf{v}_i \cdot \mathbf{v}_j) \hat{\sigma}_i \cdot \hat{\sigma}_j$, which is simply a weighted permutation operator exchanging antiparallel flavor spins i and j . The full path integral describing the propagation with $\exp[-i\hat{H}_{\nu\nu}t]$ is then a sum over all paths with all-to-all two-body spin exchanges, while the diagonal piece just reduces to pure phases, as do two-body exchanges between parallel spins.

We can write the path integral as a sum over all powers of $\hat{H}_{\nu\nu}^{\text{od}}$ operators. Summing over the number of nondiagonal operators at random times, with diagonal evolution (pure phases) between the nondiagonal terms, we can rewrite the time evolution with a path integral as

$$\begin{aligned} \langle n | \exp[-i\hat{H}_{\nu\nu}t] | \psi_0 \rangle &= \sum_m \frac{(-i)^m}{m!} \sum_{n_1 \cdots n_m} \int dt_0 \cdots dt_m \langle n | \exp[-i\hat{H}_{\nu\nu}^{\text{d}}t_m] \hat{H}_{\nu\nu}^{\text{od}} | n_m \rangle \\ &\times \langle n_m | \exp[-i\hat{H}_{\nu\nu}^{\text{d}}t_{m-1}] \hat{H}_{\nu\nu}^{\text{od}} | n_{m-1} \rangle \cdots \langle n_1 | \exp[-i\hat{H}_{\nu\nu}^{\text{d}}t_1] \hat{H}_{\nu\nu}^{\text{od}} | n_0 \rangle \langle n_0 | \psi_0 \rangle. \end{aligned} \quad (14)$$

Here, we can see that $\hat{H}_{\nu\nu}^{\text{d}}$ introduces pure phases into each term of the path integral, while the off-diagonal terms $\hat{H}_{\nu\nu}^{\text{od}}$ induce transitions from one product state to another. In this equation, the sum of all times t_i has a resultant of t , and we have separated the path integral into terms with a specific number of insertions (indexed by m) of the off-diagonal operators.

In principle, one could sample these paths by their absolute magnitudes as is done in many quantum Monte Carlo approaches, in particular diagrammatic Monte Carlo [76]. If the initial product state connects to many basis states and the $\hat{H}_{\nu\nu}^{\text{d}}$ introduces random phases, the final state is an incoherent sum of product states. The off-diagonal terms $\hat{H}_{\nu\nu}^{\text{od}}$ induce transitions as a series of spin swaps between one product state and another. Such a sampling of swaps conserves the expectation value of \hat{J}_{\pm} , \hat{J}_3 , and \hat{J}^2 of an initial product state since exchanges of the original spins have the same expectation values of total and projected spin as the original state.

All permutations of the original spins can be reached by a series of two-body swaps. For an initial product state of many neutrinos, we can easily calculate the expectation value of $\langle \hat{H}_{\nu\nu}^k \rangle$ for small k . These quantities must be conserved by the time evolution. If the angular distributions are similar, as they are deep inside a proto-neutron star, all product states of permutations of the initial spins should, when averaged over time, have equal magnitudes of overlaps A . Each permutation of the initial product state will have approximately the same $\langle \hat{H}_{\nu\nu}^{\text{d}} \rangle$, with a variance inversely proportional to the number of neutrinos since there are N^2 terms in the Hamiltonian. Unitarity requires that the average of the squared absolute magnitudes is inversely proportional to the number of spins.

More generally the time-averaged magnitudes of the amplitudes are expected to depend on the $\langle \hat{H}_{\nu\nu}^{\text{d}} \rangle$ of the individual permutations. These can arise, for example, from interference between different insertions of off-diagonal operators leading to the same final state. If we assume time-averaged overlaps vary smoothly with $\langle \hat{H}_{\nu\nu}^{\text{d}} \rangle$, we can calculate this dependence by requiring that the lowest N moments of the Hamiltonian are conserved. The linear dependence could be parametrized as a temperature as in ETH because we also know that the absolute magnitudes of the time-averaged amplitudes are real and positive. Higher-order moments put further constraints on the evolution.

Example calculations for small numbers of neutrinos are discussed below. Crucially, the low-order moments of $\hat{H}_{\nu\nu}$ can be calculated exactly from the initial product state or from an incoherent sum of physically reasonable product states.

The path integral of Eq. (14) can be described as a random walk in the basis states. For large times, we expect the phases of individual $\nu_e - \nu_{\tau}$ product states to become random if the initial product state is in the middle of the spectrum. The short time evolution of an amplitude of a particular state [$a_n(t) \equiv \langle n | \psi(t) \rangle$] up to order δt is governed by

$$\begin{aligned} a_n(t + \delta t) &= \exp[-i\hat{H}_{\nu\nu}^{\text{d}}\delta t] a_n(t) \\ &+ \sum_{m \in P(n)} \langle n | \hat{H}_{\nu\nu}^{\text{od}} | m \rangle \delta t. \end{aligned} \quad (15)$$

There are $\mathcal{O}(N^2)$ terms in the sum over states $m \in P(n)$ where $P(n)$ is the set all of the states which can be produced by one pair permutation in $\hat{H}_{\nu\nu}^{\text{od}}$, each matrix element with a substantial random component.

Assuming phases of individual $\nu_e - \nu_{\tau}$ product states at large enough time separations are random, the expression for the path integral can be described as a random walk in the basis states. The complex amplitude for a specific state at a given large time will be distributed as a two-dimensional Gaussian centered at zero describing its real and imaginary parts. The average magnitude (squared) is governed by unitarity. Integrating over times after equilibration should produce a constant absolute magnitude of the overlap, with a variance decreasing approximately inversely proportional to the square root of the time integrated over. Expectation values are obtained as the incoherent sum of expectation values in individual purely $\nu_e - \nu_{\tau}$ product states.

We investigated the behavior of the time average of $|A_n(t)|$ at late times exactly for small N . The above discussion suggests that we should expect $|A_n|_t \propto \frac{1}{\sqrt{\mathcal{N}_m}}$ where the t subscript indicates a time average and \mathcal{N}_m is the total number of states in the Hilbert space with quantum number $m = \langle n | \hat{J}_3 | n \rangle$. In Fig. 7, we show two cases. The top panel represents $\sqrt{\mathcal{N}_m} \times |A_n|_t$ for the quantum state whose one-body expectation values are shown in Figs. 4

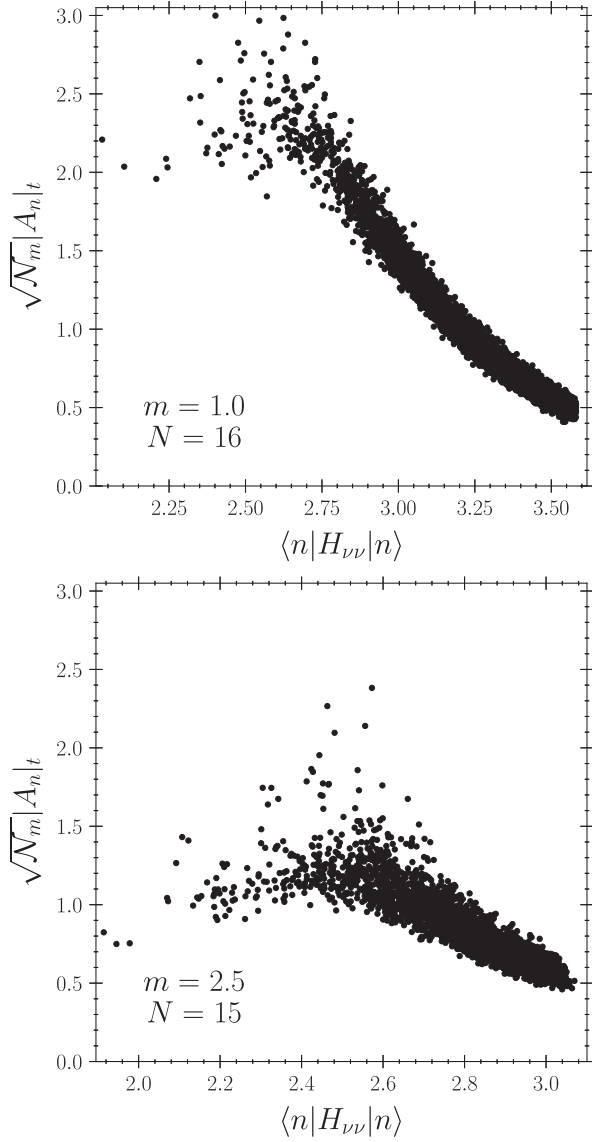


FIG. 7. Time-averaged magnitudes of state amplitudes ($|A_n|_t$) for the $N = 16$ (top) and $N = 15$ (bottom) cases in the m subspaces (top: $m = 1$, and bottom: $m = 2.5$) with the largest total overlap with the total state plotted against the respective diagonal elements of the Hamiltonian in the product state ($|n\rangle$) basis. In each case, the state projected into the specified m subspace has been normalized to unity, and the time-averaged amplitude magnitudes have been scaled by $\sqrt{\mathcal{N}_m}$, where \mathcal{N}_m is the total number of states in the specified m subspace.

and 5 for all states $|n\rangle$ in the $m = 1$ subspace, plotted against the corresponding diagonal elements of $\hat{H}_{\nu\nu}$. The lower panel is similar but for an $N = 15$ state which initially had purely $10 \nu_e$ and $5 \nu_\tau$ resulting in unit overlap with the $m = 2.5$ subspace. For the lower panel, spins were chosen as ν_e and ν_τ randomly, the $v_{x/y}$ components of velocity were chosen with random azimuthal angles on the unit sphere, and the v_z components were chosen randomly from the uniform interval $[0, 1]$.

This figure shows that for both cases, in the respective m subspaces, the time-averaged magnitudes $|A_n|_t \approx \mathcal{O}(1)/\sqrt{\mathcal{N}_m}$. Both of the considered cases show some structure in the magnitudes versus $\langle n | \hat{H}_{\nu\nu} | n \rangle$, as they must in order to conserve all of the moments of the Hamiltonian. For a more complex Hamiltonian with terms violating the conservation of J^2 or components of J or for time-varying Hamiltonians, the symmetries are further reduced [77], making the approximations considered here even more accurate. Even for the case of a specific product initial state and a static Hamiltonian with these symmetries, the behavior of the absolute magnitudes A is smooth in energy.

The equilibrium distribution in energy and angle reached by a pure neutrino system is simply the weighted average of the initial distributions in energy and angle. For the simple two-body interaction discussed here, the total number of neutrinos of each flavor is conserved. This equilibration would produce the horizontal dashed lines in Fig. 4 and is reached quite quickly, as we discussed previously.

For an incoherent sum over orthogonal states, the path integral can be modeled as a classical process including exchanges of pairs of spins. A classical swap network can be implemented for a large number of neutrinos. The potential dependence of the amplitudes on $\langle \hat{H}_{\nu\nu} \rangle$ could be implemented through a Metropolis Monte Carlo with the parametrization of the energy dependence determining the accept/reject probability. For cases with minimal dependence, such as equal initial angular distributions, the accept/reject probability could be fixed to 1.

Because of the lack of coherence, it could be that non-forward scattering would also be important. The magnitude of these amplitudes would be similar to the forward scattering. However, the phases from different magnitudes of the neutrinos' momenta would oscillate rapidly on the MeV^{-1} scale, rendering their contributions very small. In principle, all amplitudes should be consistently included and summed, but these highly oscillatory pieces are unlikely to significantly interfere with the forward scattering amplitudes. The same picture of random diagonal phases and rapid flavor exchanges would occur and not change this picture, particularly since the angular dependence is not measurable. At larger distances where the neutrino flux is reduced, off-diagonal vacuum oscillation terms will be important, leading to further flavor evolution. Potentially, this could be modeled as a system of single neutrino spins evolving according to their one-body Hamiltonian with random swaps imposed. However, the equilibrium we discuss should dominate at smaller radii where much of the dynamics and chemical evolution occurs. At larger radii, the evolution is governed by simple one-body dynamics due to the expected geometric reduction in the strength of the two-body interaction.

The case of a mixture of neutrinos and antineutrinos of different flavors is more interesting. The total number density of a particular flavor of neutrino (or antineutrino) is denoted by $n(\nu_x)$, and the net lepton flavor is given by

$n(\nu_x) - n(\bar{\nu}_x)$. The net lepton number is preserved by the path integral picture with random phases and two-particle exchanges. The net lepton flavor for each flavor is conserved by the evolution which provides 3 conservation conditions and the total number of neutrinos is also conserved which provides a fourth condition. However, the total number of neutrinos and antineutrinos in each flavor must be known to specify the full equilibrium distribution, thus requiring a total of six values to be specified. Assuming random phases renders the quantum problem essentially classical, and then it is possible to determine the equilibrium distributions very easily.

Assume that the flavor swapping processes $\nu_e(\mathbf{p}) + \nu_x(\mathbf{p}') \rightleftharpoons \nu_e(\mathbf{p}') + \nu_x(\mathbf{p})$ have achieved equilibrium. Because the forward and reverse processes have the same scattering amplitude, one must have $n_{\nu_e}(\mathbf{p})n_{\nu_x}(\mathbf{p}') = n_{\nu_e}(\mathbf{p}')n_{\nu_x}(\mathbf{p})$ or, equivalently, $n_{\nu_e}(\mathbf{p})/n_{\nu_x}(\mathbf{p}) = n_{\nu_e}(\mathbf{p}')/n_{\nu_x}(\mathbf{p}') = q$. Therefore, the ν_e to ν_x ratio is independent of the neutrino momentum when the flavor equilibrium is obtained. Similarly, one also has $n_{\nu_e}(\mathbf{p})/n_{\nu_x}(\mathbf{p}) = n_{\bar{\nu}_e}(\mathbf{p}')/n_{\bar{\nu}_x}(\mathbf{p}') = q$ if $\nu_e(\mathbf{p}) + \bar{\nu}_e(\mathbf{p}') \rightleftharpoons \nu_x(\mathbf{p}) + \bar{\nu}_x(\mathbf{p}')$ have reached equilibrium. This is consistent with the flavor isospin notation where the antineutrinos are treated as neutrinos with negative energies [78]. Using the constancy of q , one can determine the equilibrium distribution completely for given $n(\nu_e) - n(\bar{\nu}_e)$ and $n(\nu_x) - n(\bar{\nu}_x)$.

In environments where both neutrinos and antineutrinos are present, flavor off-diagonal evolution from processes like $\nu_e\bar{\nu}_e \rightleftharpoons \nu_\mu\bar{\nu}_\mu$ yields a rapid equilibrium. In such an equilibrium state, the time-averaged flux into a particular state must equal the time-averaged flux out of a state. Since the magnitude of the Hamiltonian matrix elements are symmetric under time reversal, this implies the probability of the product of the densities of neutrinos and antineutrinos in each flavor must satisfy $n(\nu_e)n(\bar{\nu}_e) = n(\nu_\mu)n(\bar{\nu}_\mu) = n(\nu_\tau)n(\bar{\nu}_\tau)$, where n represents the density of neutrinos of a given flavor. These two additional conditions on the product of neutrino and antineutrino densities, along with the four previous, completely determine the equilibrium condition.

We consider a simply implemented three-neutrino-flavor swap network of 24,000 total neutrinos and antineutrinos, each labeled only by their energy, as we expect that the flavor evolution will rapidly tend to isotropy in momentum given the above arguments. We distribute them randomly in energy with a distribution that mimics an energy weighted Boltzmann distribution of the form $\mathcal{P}(E) \propto Ee^{-\beta E}$ which we show in the top panels for all neutrino and antineutrino species in Fig. 8. We start with initial distributions with fractional $n(\nu_e) = 1/2$ and an average energy of 11.9 MeV, $n(\bar{\nu}_e) = 1/6$ with an average energy of 15 MeV and all other species with $n(\nu_x) = 1/12$ and an average energy of 18.2 MeV.

With these initial populations, we perform swaps among the neutrinos and antineutrinos of different energies by

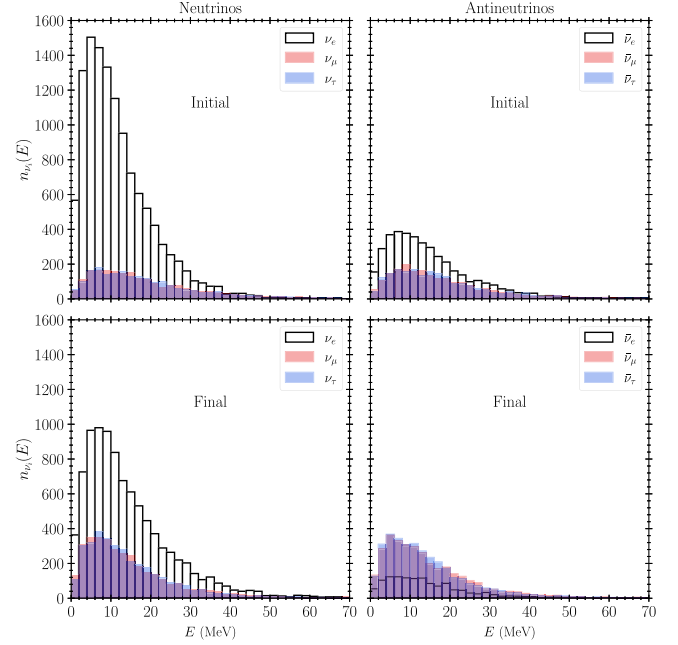


FIG. 8. Initial (top) and final (bottom) neutrino energy spectra ($n_{\nu_i}(E)$) for each flavor (denoted i) in a simple calculation assuming random phases from the diagonal parts of the Hamiltonian. The product of the number of electron neutrinos and antineutrinos equilibrates with the other flavors, while the difference is maintained for each flavor.

randomly selecting two neutrinos from the distribution and swapping their energies. In this process, if a neutrino and antineutrino of the same type are selected, we also allow them to change to a different flavor, with probability $\frac{1}{3}$ for each flavor. We perform this swapping process on average 250 times per neutrino in the distribution, and we show the final flavor configuration after the swap network in the two lower panels of Fig. 8.

For the swapped distribution, we find that the average energy of each species is approximately equal and is $\bar{E} \approx 14.5$ MeV. The numbers of electron flavor neutrinos and antineutrinos are reduced to 0.38 and 0.05, respectively, by transformation to other flavors with equal products of number of neutrinos times antineutrinos in all flavors. The other flavor populations are increased slightly to 0.14. While the individual flavor populations have been adjusted, the conserved differences have been respected. This rapid approach to equilibrium can significantly impact the dynamics and chemical evolution of supernovae and neutron star mergers.

IV. CONCLUSION

In this work, we have provided evidence that the generic $\nu - \nu$ coherent forward scattering Hamiltonian is nonintegrable, and the resultant level spacing statistics behave equivalently to those of a random matrix drawn from a Gaussian orthogonal ensemble. This behavior is generically expected

in nonintegrable Hamiltonians as there is not an extensive set of conserved quantities which would admit degeneracy in the spectrum. Such Hamiltonians display chaotic behavior, and a large category of initial conditions is expected to thermalize in the sense that one-body expectation values will obtain some equilibrium value from which they stray only transiently and which can be predicted from an energy diagonal grand-canonical thermal distribution.

Artificial impositions of symmetry can categorically change the nature of the coherent forward scattering Hamiltonian. We should only make such simplifying assumptions in the pursuit of understanding if doing so does not qualitatively change the behavior of the system we are studying. This work strongly encourages more careful consideration on how to appropriately take a thermodynamic limit in these systems.

The evidence we present here strongly suggests that late-time one-body expectation values can be obtained *a priori* from a thermal partition function. While fully diagonalizing the Hamiltonian for large N is prohibitively expensive, even in the lower-dimensional block-decimated invariant subspaces, Monte Carlo methods may be feasibly implemented to evaluate the partition function at larger values of N . Such a scheme may provide a method for feasibly determining the late-time one-body flavor expectation values in the fast oscillation regime without explicitly solving the many-body Schrödinger equation or numerically diagonalizing the Hamiltonian.

While the time-independent Hamiltonian and initial conditions we consider here are quite simple, we do not expect the neglected effects, including nonforward scattering, spatially resolved initial states, or time dependence in the Hamiltonian, to fundamentally increase the coherence in the system. In at least some cases, a simple classical picture of equilibrium, as determined by assuming an evolution to an incoherent sum of product states, should provide an accurate approximation to one-body observables. In particular, this path integral picture can be used to define an intriguing equilibrium distribution for systems of neutrinos and antineutrinos of multiple flavors.

Furthermore, in the near future, quantum computers may provide an avenue for performing the coherent time evolution of the quantum many-body system (see, e.g., Refs. [44,79–83] for recent attempts on current generation devices) and may be capable of evaluating expectation values using explicit time evolution for similarly large N , which can be compared to statistical partition functions obtained on either classical or quantum computers. As such, quantum computers may facilitate comparisons between these two predictions.

Finally, as the number of spins included increases, the block-decimated subspaces of the Hamiltonian grow combinatorially large, which we should expect to drive the system even closer to the predictions made utilizing the partition function. While we have provided evidence which

suggests that the equilibration we have observed here will be obtained when $\hat{H}_{\nu\nu}$ dominates the evolution, a remaining open question is the precise rate at which this thermal equilibrium is achieved. We generally observe equilibration on a timescale which is on the order of $\sim 10\mu^{-1}$; however, we have not proven that this will occur on such short timescales generically. The examples we have studied do not display sufficient sensitivity to the system size in the equilibration timescale to make a clear determination of the relationship. We leave a more thorough investigation of the approach to equilibrium to future work.

ACKNOWLEDGMENTS

We thank Vincenzo Cirigliano, Ivan Deutsch, and George Fuller for productive conversations. This work was supported by the Quantum Science Center (QSC), a National Quantum Information Science Research Center of the U.S. Department of Energy (DOE), and by the U.S. Department of Energy, Office of Science, Office of Nuclear Physics (NP) Contract No. DE-AC52-06NA25396. H. D. is supported by the U.S. DOE NP Grant No. DE-SC0017803 at UNM.

APPENDIX: SHORT TIME EVOLUTION

An important question to address is when equilibration is reached for a given initial state. A simple approach is to Taylor expand the time evolution of the operator in the given initial state and use the expansion to estimate when the first crossing of the equilibrium value is reached, as depicted in Fig. 5. In what follows, we will refer to the flavor state of a given neutrino simply as the state of a given site in our system. We introduce the swap operator $\hat{\rho}_{ij} = \frac{1}{2}\hat{\sigma}_i \cdot \hat{\sigma}_j + \frac{1}{2}$, whose action on a tensor product state of sites i and j and any other state representing the rest of the system is given by

$$\hat{\rho}_{ij}|a\rangle_i \otimes |b\rangle_j \otimes |\psi\rangle = |b\rangle_i \otimes |a\rangle_j \otimes |\psi\rangle. \quad (\text{A1})$$

We can take our Hamiltonian of Eq. (1) and rewrite it as (up to a term proportional to the identity)

$$\hat{H}_{\nu\nu} = \frac{1}{N} \sum_{i<j}^N \mu_{ij} \hat{\rho}_{ij}, \quad (\text{A2})$$

where we introduce the variables $\mu_{ij} = \mu(1 - \mathbf{v}_i \cdot \mathbf{v}_j)$ for conciseness.

Working in the Heisenberg picture, we then can calculate the time evolution of a Pauli matrix at a site i , which we fix for definiteness to be in the \vec{e}_3 direction and choose $i = 1$, though our results do not depend on these choices:

$$\begin{aligned} \hat{\sigma}_{3,1}(t) &= e^{-i\hat{H}_{\nu\nu}t} \hat{\sigma}_{3,1} e^{i\hat{H}_{\nu\nu}t} \\ &= \hat{\sigma}_{3,1} - it[\hat{H}_{\nu\nu}, \hat{\sigma}_{3,1}] + \frac{(it)^2}{2} [\hat{H}_{\nu\nu}, [\hat{H}_{\nu\nu}, \hat{\sigma}_{3,1}]] + \dots \end{aligned} \quad (\text{A3})$$

To compute these commutators, we note the following identity:

$$[\hat{H}_{\nu\nu}, \hat{P} \cdot \hat{\sigma}_{3,k}] = \sum_{i < j}^N \frac{\mu_{ij}}{N} (\hat{\rho}_{ij} \hat{P} \hat{\sigma}_{3,k} - \hat{P} \hat{\rho}_{ij} \hat{\sigma}_{3,\rho_{ij}(k)}) \quad (\text{A4})$$

$$\text{with index: } \rho_{ij}(k) = \begin{cases} j & \text{if } k = i, \\ i & \text{if } k = j, \\ k & \text{else.} \end{cases} \quad (\text{A5})$$

$$[\hat{H}_{\nu\nu}, \hat{\sigma}_{3,1}] = \sum_{1 < j \leq N} \frac{\mu_{1j}}{N} \hat{\rho}_{1j} (\hat{\sigma}_{3,1} - \hat{\sigma}_{3,j}), \quad (\text{A7})$$

$$\begin{aligned} [\hat{H}_{\nu\nu}, [\hat{H}_{\nu\nu}, \hat{\sigma}_{3,1}]] &= \frac{1}{N^2} \sum_{1 < j \leq N} \sum_{\ell \neq 1, j} \{ \mu_{1j} \mu_{j\ell} (\hat{\rho}_{1j\ell} (\hat{\sigma}_{3,1} - \hat{\sigma}_{3,j}) - \hat{\rho}_{1\ell j} (\hat{\sigma}_{3,1} - \hat{\sigma}_{3,\ell})) \\ &\quad + \mu_{1j} \mu_{1\ell} (\hat{\rho}_{1j\ell} (\hat{\sigma}_{3,1} - \hat{\sigma}_{3,j}) - \hat{\rho}_{1\ell j} (\hat{\sigma}_{3,j} - \hat{\sigma}_{3,\ell})) \} + 2 \sum_{1 < j \leq N} \frac{\mu_{1j}^2}{N^2} (\hat{\sigma}_{3,1} - \hat{\sigma}_{3,j}). \end{aligned} \quad (\text{A8})$$

The operators of the form $\hat{\rho}_{ijk} \equiv \hat{\rho}_{ik} \hat{\rho}_{ij}$ are cyclic permutations, mapping states as from site i to j , site j to k , and site k to i .

Using the operator norm (the largest absolute value of the eigenvalues in the operator, $\|\hat{O}\| = \sup_{\psi} |\langle \psi | \hat{O} | \psi \rangle|$), we can bound how large the expectation values are for any given state using the triangle inequality and submultiplicativity of the norm:

$$\|\hat{A} + \hat{B}\| \leq \|\hat{A}\| + \|\hat{B}\|, \quad (\text{A9})$$

$$\|\hat{A} \hat{B}\| \leq \|\hat{A}\| \|\hat{B}\|, \quad (\text{A10})$$

to get

$$\|[\hat{H}_{\nu\nu}, \hat{\sigma}_{3,1}]\| \leq 2 \sum_{1 < j \leq N} \frac{\mu_{1j}}{N} \sim \mathcal{O}(\mu), \quad (\text{A11})$$

$$\begin{aligned} \|[\hat{H}_{\nu\nu}, [\hat{H}_{\nu\nu}, \hat{\sigma}_{3,1}]]\| &\leq \frac{4}{N^2} \sum_{1 < j \leq N} \left\{ \mu_{1j}^2 + \sum_{\ell \neq 1, j} (\mu_{1j} \mu_{j\ell} + \mu_{1j} \mu_{1\ell}) \right\} \\ &\sim \mathcal{O}(\mu^2). \end{aligned} \quad (\text{A12})$$

These represent the *worst/best* case scenario for the expectation value of these operators, that is, the largest values the coefficients of the Taylor expansion can take. However, a given state may or may not have an expectation value with the same asymptotic behavior in the limit that $N \gg 1$ as our upper bounds. To see this, we consider the product state with ± 1 states at all sites, polarized along the \vec{e}_3 axis:

Here, \hat{P} is an extended permutation operator built from a product of multiple swaps, and we have shifted our Pauli matrix to operate on another site using:

$$\hat{\sigma}_{3,k} \hat{\rho}_{ij} = \hat{\rho}_{ij} \hat{\sigma}_{3,\rho_{ij}(k)}. \quad (\text{A6})$$

This allows us to express the commutators as a sum over permutations times a Pauli matrix. We then compute

$$|m_+, m_-\rangle = \underbrace{|1, \dots, 1\rangle}_{m_+ \text{ times}} \underbrace{|-1, \dots, -1\rangle}_{m_- \text{ times}}. \quad (\text{A13})$$

There is nothing special about this product state in this basis; any permutation of the sites states will lead to the same conclusions in what follows. We can quickly see

$$\langle m_+, m_- | [\hat{H}_{\nu\nu}, \hat{\sigma}_{3,1}] | m_+, m_- \rangle = 0. \quad (\text{A14})$$

The swap operator forces the states at sites 1 and j to be identical, but then the expectation values of the Pauli matrices at those sites are also identical. Similarly, we compute

$$\begin{aligned} \langle m_+, m_- | [\hat{H}_{\nu\nu}, [\hat{H}_{\nu\nu}, \hat{\sigma}_{3,1}]] | m_+, m_- \rangle &= 4 \sum_{j, |\phi|_j = |-1\rangle} \frac{\mu_{1j}^2}{N^2} \\ &\sim \mathcal{O}\left(\frac{\mu^2 m_-}{N^2}\right). \end{aligned} \quad (\text{A15})$$

The contribution from the first two lines of Eq. (A8) is zero, term by term in the sums. The permutation operators force the states to be identical at the permuting sites, but then the expectation value of the Pauli matrices must cancel.

In general, moving beyond a single flavor polarized product state, we can extend these conclusions to the class of states that have random phases when written in the computational basis of product states of $|\pm 1\rangle$. The expectation value becomes approximately diagonal in the product states, with positive coefficients bounded by 1 from unitarity, so for such states, we can expect

$$\langle \psi | [\hat{H}_{\nu\nu}, \hat{\sigma}_{3,1}] | \psi \rangle \sim 0, \quad \text{and} \quad (\text{A16})$$

$$\langle \psi | [\hat{H}_{\nu\nu}, [\hat{H}_{\nu\nu}, \hat{\sigma}_{3,1}]] | \psi \rangle \sim \mathcal{O}\left(\frac{\mu^2}{N}\right). \quad (\text{A17})$$

In the second line, we assume that the product states generically have $\mathcal{O}(N) | + 1 \rangle$ -polarized states and/or $\mathcal{O}(N) | - 1 \rangle$ -polarized states. Clearly, they cannot exceed this.

-
- [1] H. A. Bethe, Supernova mechanisms, *Rev. Mod. Phys.* **62**, 801 (1990).
- [2] James Pantaleone, Neutrino oscillations at high densities, *Phys. Lett. B* **287**, 128 (1992).
- [3] Hans-Thomas Janka, K. Langanke, A. Marek, G. Martinez-Pinedo, and B. Mueller, Theory of core-collapse supernovae, *Phys. Rep.* **442**, 38 (2007).
- [4] Stan Woosley and Thomas Janka, The physics of core-collapse supernovae, *Nat. Phys.* **1**, 147 (2005).
- [5] R. D. Hoffman, S. E. Woosley, and Y. Z. Qian, Nucleosynthesis in neutrino driven winds. II. Implications for heavy element synthesis, *Astrophys. J.* **482**, 951 (1997).
- [6] Xinyu Li and Daniel M. Siegel, Neutrino fast flavor conversions in neutron-star postmerger accretion disks, *Phys. Rev. Lett.* **126**, 251101 (2021).
- [7] Rodrigo Fernández, Sherwood Richers, Nicole Mulyk, and Steven Fahlman, Fast flavor instability in hypermassive neutron star disk outflows, *Phys. Rev. D* **106**, 103003 (2022).
- [8] G. Sigl and G. Raffelt, General kinetic description of relativistic mixed neutrinos, *Nucl. Phys.* **B406**, 423 (1993).
- [9] Yong Zhong Qian and George M. Fuller, Neutrino-neutrino scattering and matter enhanced neutrino flavor transformation in supernovae, *Phys. Rev. D* **51**, 1479 (1995).
- [10] Yong-Zhong Qian and George M. Fuller, Matter-enhanced antineutrino flavor transformation and supernova nucleosynthesis, *Phys. Rev. D* **52**, 656 (1995).
- [11] Sergio Pastor and Georg Raffelt, Flavor oscillations in the supernova hot bubble region: Nonlinear effects of neutrino background, *Phys. Rev. Lett.* **89**, 191101 (2002).
- [12] Sergio Pastor, Georg Raffelt, and Dmitry V. Semikoz, Physics of synchronized neutrino oscillations caused by self-interactions, *Phys. Rev. D* **65**, 053011 (2002).
- [13] Nicole F. Bell, Andrew A. Rawlinson, and R. F. Sawyer, Speedup through entanglement: Many body effects in neutrino processes, *Phys. Lett. B* **573**, 86 (2003).
- [14] R. F. Sawyer, ‘Classical’ instabilities and ‘quantum’ speed-up in the evolution of neutrino clouds, [arXiv:hep-ph/0408265](https://arxiv.org/abs/hep-ph/0408265).
- [15] A. B. Balantekin and Y. Pehlivan, Neutrino-neutrino interactions and flavor mixing in dense matter, *J. Phys. G* **34**, 47 (2007).
- [16] Huaiyu Duan, George M. Fuller, J. Carlson, and Yong-Zhong Qian, Coherent development of neutrino flavor in the supernova environment, *Phys. Rev. Lett.* **97**, 241101 (2006).
- [17] Georg G. Raffelt and Alexei Yu. Smirnov, Self-induced spectral splits in supernova neutrino fluxes, *Phys. Rev. D* **76**, 081301 (2007); **77**, 029903(E) (2008).
- [18] Georg G. Raffelt and Alexei Yu. Smirnov, Adiabaticity and spectral splits in collective neutrino transformations, *Phys. Rev. D* **76**, 125008 (2007).
- [19] R. F. Sawyer, Speed-up of neutrino transformations in a supernova environment, *Phys. Rev. D* **72**, 045003 (2005).
- [20] R. F. Sawyer, Multiangle instability in dense neutrino systems, *Phys. Rev. D* **79**, 105003 (2009).
- [21] R. F. Sawyer, Neutrino cloud instabilities just above the neutrino sphere of a supernova, *Phys. Rev. Lett.* **116**, 081101 (2016).
- [22] Sovan Chakraborty, Rasmus Sloth Hansen, Ignacio Izaguirre, and Georg G. Raffelt, Self-induced neutrino flavor conversion without flavor mixing, *J. Cosmol. Astropart. Phys.* **03** (2016) 042.
- [23] Ignacio Izaguirre, Georg Raffelt, and Irene Tamborra, Fast pairwise conversion of supernova neutrinos: A dispersion relation approach, *Phys. Rev. Lett.* **118**, 021101 (2017).
- [24] Basudeb Dasgupta, Alessandro Mirizzi, and Manibrata Sen, Fast neutrino flavor conversions near the supernova core with realistic flavor-dependent angular distributions, *J. Cosmol. Astropart. Phys.* **02** (2017) 019.
- [25] Meng-Ru Wu and Irene Tamborra, Fast neutrino conversions: Ubiquitous in compact binary merger remnants, *Phys. Rev. D* **95**, 103007 (2017).
- [26] Sajad Abbar and Huaiyu Duan, Fast neutrino flavor conversion: Roles of dense matter and spectrum crossing, *Phys. Rev. D* **98**, 043014 (2018).
- [27] Basudeb Dasgupta, Alessandro Mirizzi, and Manibrata Sen, Simple method of diagnosing fast flavor conversions of supernova neutrinos, *Phys. Rev. D* **98**, 103001 (2018).
- [28] Sagar Airen, Francesco Capozzi, Sovan Chakraborty, Basudeb Dasgupta, Georg Raffelt, and Tobias Stirner, Normal-mode analysis for collective neutrino oscillations, *J. Cosmol. Astropart. Phys.* **12** (2018) 019.
- [29] Joshua D. Martin, Changhao Yi, and Huaiyu Duan, Dynamic fast flavor oscillation waves in dense neutrino gases, *Phys. Lett. B* **800**, 135088 (2020).
- [30] Lucas Johns, Hiroki Nagakura, George M. Fuller, and Adam Burrows, Neutrino oscillations in supernovae: Angular moments and fast instabilities, *Phys. Rev. D* **101**, 043009 (2020).
- [31] Alessandro Roggero, Ermal Rrapaj, and Zewei Xiong, Entanglement and correlations in fast collective neutrino flavor oscillations, *Phys. Rev. D* **106**, 043022 (2022).
- [32] Soumya Bhattacharyya and Basudeb Dasgupta, Elaborating the ultimate fate of fast collective neutrino flavor oscillations, *Phys. Rev. D* **106**, 103039 (2022).

- [33] Zewei Xiong and Yong-Zhong Qian, Stationary solutions for fast flavor oscillations of a homogeneous dense neutrino gas, *Phys. Lett. B* **820**, 136550 (2021).
- [34] Maria Cristina Volpe, Neutrinos from dense: Flavor mechanisms, theoretical approaches, observations, new directions, [arXiv:2301.11814](https://arxiv.org/abs/2301.11814).
- [35] L. Wolfenstein, Neutrino oscillations in matter, *Phys. Rev. D* **17**, 2369 (1978).
- [36] S. P. Mikheev and A. Yu. Smirnov, Resonance amplification of oscillations in matter and spectroscopy of solar neutrinos, *Yad. Fiz.* **42**, 1441 (1985).
- [37] Alexander Friedland, Bruce H. J. McKellar, and Ivona Okuniewicz, Construction and analysis of a simplified many-body neutrino model, *Phys. Rev. D* **73**, 093002 (2006).
- [38] Bruce H. J. McKellar, Ivona Okuniewicz, and James Quach, Non-Boltzmann behavior in models of interacting neutrinos, *Phys. Rev. D* **80**, 013011 (2009).
- [39] Y. Pehlivan, A. B. Balantekin, Toshitaka Kajino, and Takashi Yoshida, Invariants of collective neutrino oscillations, *Phys. Rev. D* **84**, 065008 (2011).
- [40] Savas Birol, Y. Pehlivan, A. B. Balantekin, and T. Kajino, Neutrino spectral split in the exact many body formalism, *Phys. Rev. D* **98**, 083002 (2018).
- [41] Amol V. Patwardhan, Michael J. Cervia, and A. Baha Balantekin, Eigenvalues and eigenstates of the many-body collective neutrino oscillation problem, *Phys. Rev. D* **99**, 123013 (2019).
- [42] Amol V. Patwardhan, Michael J. Cervia, and A. B. Balantekin, Spectral splits and entanglement entropy in collective neutrino oscillations, *Phys. Rev. D* **104**, 123035 (2021).
- [43] Joshua D. Martin, A. Roggero, Huaiyu Duan, J. Carlson, and V. Cirigliano, Classical and quantum evolution in a simple coherent neutrino problem, *Phys. Rev. D* **105**, 083020 (2022).
- [44] Marc Illa and Martin J. Savage, Multi-neutrino entanglement and correlations in dense neutrino systems, *Phys. Rev. Lett.* **130**, 221003 (2023).
- [45] Zewei Xiong, Many-body effects of collective neutrino oscillations, *Phys. Rev. D* **105**, 103002 (2022).
- [46] Shashank Shalgar and Irene Tamborra, Do we have enough evidence to invalidate the mean-field approximation adopted to model collective neutrino oscillations?, *Phys. Rev. D* **107**, 123004 (2023).
- [47] Ermal Rrapaj, Exact solution of multiangle quantum many-body collective neutrino-flavor oscillations, *Phys. Rev. C* **101**, 065805 (2020).
- [48] Alessandro Roggero, Entanglement and many-body effects in collective neutrino oscillations, *Phys. Rev. D* **104**, 103016 (2021).
- [49] Alessandro Roggero, Dynamical phase transitions in models of collective neutrino oscillations, *Phys. Rev. D* **104**, 123023 (2021).
- [50] Denis Lacroix, A. B. Balantekin, Michael J. Cervia, Amol V. Patwardhan, and Pooja Siwach, Role of non-Gaussian quantum fluctuations in neutrino entanglement, *Phys. Rev. D* **106**, 123006 (2022).
- [51] Michael J. Cervia, Amol V. Patwardhan, A. B. Balantekin, S. N. Coppersmith, and Calvin W. Johnson, Entanglement and collective flavor oscillations in a dense neutrino gas, *Phys. Rev. D* **100**, 083001 (2019).
- [52] Damiano F. G. Fiorillo and Georg G. Raffelt, Slow and fast collective neutrino oscillations: Invariants and reciprocity, *Phys. Rev. D* **107**, 043024 (2023).
- [53] Lucas Johns, Neutrino many-body correlations, [arXiv:2305.04916](https://arxiv.org/abs/2305.04916).
- [54] Jasen A. Scaramazza, B. Sriram Shastry, and Emil A. Yuzbashyan, Integrable matrix theory: Level statistics, *Phys. Rev. E* **94**, 032106 (2016).
- [55] Y. Y. Atas, Eugene Bogomolny, O. Giraud, and G. Roux, Distribution of the ratio of consecutive level spacings in random matrix ensembles, *Phys. Rev. Lett.* **110**, 084101 (2013).
- [56] J. M. Deutsch, Quantum statistical mechanics in a closed system, *Phys. Rev. A* **43**, 2046 (1991).
- [57] Mark Srednicki, Chaos and quantum thermalization, *Phys. Rev. E* **50**, 888 (1994).
- [58] Mark Srednicki, Thermal fluctuations in quantized chaotic systems, *J. Phys. A* **29**, L75 (1996).
- [59] Luca D'Alessio, Yariv Kafri, Anatoli Polkovnikov, and Marcos Rigol, From quantum chaos and eigenstate thermalization to statistical mechanics and thermodynamics, *Adv. Phys.* **65**, 239 (2016).
- [60] Marcos Rigol, Quantum quenches and thermalization in one-dimensional fermionic systems, *Phys. Rev. A* **80**, 053607 (2009).
- [61] Marcos Rigol and Lea F. Santos, Quantum chaos and thermalization in gapped systems, *Phys. Rev. A* **82**, 011604 (2010).
- [62] Hyungwon Kim, Tatsuhiko N. Ikeda, and David A. Huse, Testing whether all eigenstates obey the eigenstate thermalization hypothesis, *Phys. Rev. E* **90**, 052105 (2014).
- [63] C. L. Baldwin, C. R. Laumann, A. Pal, and A. Scardicchio, Clustering of nonergodic eigenstates in quantum spin glasses, *Phys. Rev. Lett.* **118**, 127201 (2017).
- [64] Patrycja Łydźba, Yicheng Zhang, Marcos Rigol, and Lev Vidmar, Single-particle eigenstate thermalization in quantum-chaotic quadratic Hamiltonians, *Phys. Rev. B* **104**, 214203 (2021).
- [65] David Villaseñor, Saúl Pilatowsky-Cameo, Miguel A. Bastarrachea-Magnani, Sergio Lerma-Hernández, Lea F. Santos, and Jorge G. Hirsch, Chaos and thermalization in the spin-boson Dicke model, *Entropy* **25**, 8 (2022).
- [66] Naoto Shiraishi and Takashi Mori, Systematic construction of counterexamples to the eigenstate thermalization hypothesis, *Phys. Rev. Lett.* **119**, 030601 (2017).
- [67] Kiryl Pakrouski, Preethi N. Pallegar, Fedor K. Popov, and Igor R. Klebanov, Many-body scars as a group invariant sector of Hilbert space, *Phys. Rev. Lett.* **125**, 230602 (2020).
- [68] Nicolas Regnault, Sanjay Moudgalya, and B. Andrei Bernevig, Quantum many-body scars and Hilbert space fragmentation: A review of exact results, *Rep. Prog. Phys.* **85**, 086501 (2022).
- [69] Mark Srednicki, The approach to thermal equilibrium in quantized chaotic systems, *J. Phys. A* **32**, 1163 (1999).
- [70] Daniel E. Parker, Xiangyu Cao, Alexander Avdoshkin, Thomas Scaffidi, and Ehud Altman, A universal operator growth hypothesis, *Phys. Rev. X* **9**, 041017 (2019).

- [71] Chaitanya Murthy and Mark Srednicki, Bounds on chaos from the eigenstate thermalization hypothesis, *Phys. Rev. Lett.* **123**, 230606 (2019).
- [72] Ehsan Khatami, Guido Pupillo, Mark Srednicki, and Marcos Rigol, Fluctuation-dissipation theorem in an isolated system of quantum dipolar bosons after a quench, *Phys. Rev. Lett.* **111**, 050403 (2013).
- [73] Chaitanya Murthy, Arman Babakhani, Fernando Iniguez, Mark Srednicki, and Nicole Yunger Halpern, Non-Abelian eigenstate thermalization hypothesis, *Phys. Rev. Lett.* **130**, 140402 (2023).
- [74] Vittorio Giovannetti, Seth Lloyd, and Lorenzo Maccone, Quantum limits to dynamical evolution, *Phys. Rev. A* **67**, 052109 (2003).
- [75] Martha Gutiérrez and Arseni Goussev, Long-time saturation of the Loschmidt echo in quantum chaotic billiards, *Phys. Rev. E* **79**, 046211 (2009).
- [76] Kris Van Houcke, Evgeny Kozik, N. Prokof'ev, and B. Svistunov, Diagrammatic Monte Carlo, *Phys. Procedia* **6**, 95 (2010).
- [77] Joshua D. Martin, A. Roggero, Huaiyu Duan, and J. Carlson, Many-body neutrino flavor entanglement in a simple dynamic model, [arXiv:2301.07049](https://arxiv.org/abs/2301.07049).
- [78] Huaiyu Duan, George M. Fuller, and Yong-Zhong Qian, Collective neutrino flavor transformation in supernovae, *Phys. Rev. D* **74**, 123004 (2006).
- [79] Benjamin Hall, Alessandro Roggero, Alessandro Baroni, and Joseph Carlson, Simulation of collective neutrino oscillations on a quantum computer, *Phys. Rev. D* **104**, 063009 (2021).
- [80] Kübra Yeter-Aydeniz, Shikha Bangar, George Siopsis, and Raphael C. Pooser, Collective neutrino oscillations on a quantum computer, *Quantum Inf. Process.* **21**, 84 (2022).
- [81] Marc Illa and Martin J. Savage, Basic elements for simulations of standard-model physics with quantum annealers: Multigrid and clock states, *Phys. Rev. A* **106**, 052605 (2022).
- [82] Valentina Amitrano, Alessandro Roggero, Piero Luchi, Francesco Turro, Luca Vespucci, and Francesco Pederiva, Trapped-ion quantum simulation of collective neutrino oscillations, *Phys. Rev. D* **107**, 023007 (2023).
- [83] Pooja Siwach, Kaytlin Harrison, and A. Baha Balantekin, Collective neutrino oscillations on a quantum computer with hybrid quantum-classical algorithm, *Phys. Rev. D* **108**, 083039 (2023).